Tunable thermoelectric properties in bended graphene nanoribbons*

Chang-Ning Pan(潘长宁)[1], Jun He(何军)[1,†], and Mao-Fa Fang(方卯发)[2]

[1] School of Science, Hunan University of Technology, Zhuzhou 412008, China
[2] Key Laboratory of Low-Dimensional Quantum Structures and Quantum Control of Ministry of Education and Department of Physics, Hunan Normal University, Changsha 410081, China

(Received 1 February 2016; revised manuscript received 25 March 2016; published online 1 June 2016)

The ballistic thermoelectric properties in bended graphene nanoribbons (GNRs) are systematically investigated by using atomistic simulation of electron and phonon transport. We find that the electron resonant tunneling effect occurs in the metallic–semiconducting linked ZZ-GNRs (the bended GNRs with zigzag edge leads). The electron-wave quantum interference effect occurs in the metallic–metallic linked AA-GNRs (the bended GNRs with armchair edge leads). These different physical mechanisms lead to the large Seebeck coefficient S and high electron conductance in bended ZZ-GNRs/AA-GNRs. Combined with the reduced lattice thermal conduction, the significant enhancement of the figure of merit ZT is predicted. Moreover, we find that the ZT_{max} (the maximum peak of ZT) is sensitive to the structural parameters. It can be conveniently tuned by changing the interbend length of bended GNRs. The magnitude of ZT ranges from the 0.15 to 0.72. Geometry-controlled ballistic thermoelectric effect offers an effective way to design thermoelectric devices such as thermocouples based on graphene.

Keywords: graphene nanoribbons, thermoelectric properties, quantum interference effect

PACS: 81.05.U–, 73.63.–b, 72.20.Pa **DOI:** 10.1088/1674-1056/25/7/078102

1. Introduction

The discovery of two-dimensional graphene and quasi-one-dimensional graphene nanoribbons (GNRs) has attracted great interest due to its fascinating physical properties and potential applications in nanoelectronics, photonics, spintronics, and optoelectronics.[1,2] In particular, with the increase in energy demand, more and more attention has been focused on the thermoelectric properties of graphene structures, which can convert directly temperature gradients to electric voltage, and vice versa. The thermoelectric effect can be quantified by the dimensionless figure of merit

$$\mathrm{ZT} = \frac{TG_{\mathrm{e}}S^2}{\kappa_{\mathrm{e}} + \kappa_{\mathrm{ph}}}, \tag{1}$$

where T is the average temperature, G_{e} is the electronic conductance, S is the Seebeck coefficient, κ_{e} is the electron thermal conductance, and κ_{ph} is the phonon thermal conductance, respectively. In recent years, the optimization of thermoelectric properties has become a hot topic of nanostructured materials,[3–8] and many ways have been proposed in previous researches. One approach is to increase the Seebeck coefficient S by reducing the dimensionality of the system,[9] i.e., the quantum confinement effect of electrons can strengthen the Seebeck coefficient.[10] Another idea is to decrease the phonon thermal conductivity by the structure modulation while the high electronic conductance is kept unchanged by the resonant tunneling of electrons in nanostructured materials.[11]

In practice, the pristine GNRs with the thermoelectronic figure of merit ZT ~ 0.01 are always considered to be inefficient thermoelectric materials and cannot be directly applied in the thermoelectric conversion, although such high Seebeck coefficients have been found in such systemss.[12] The main reason is that the perfect graphene have superior thermal conductivity. Hence, many methods have already been examined to reduce the thermal conductivity and then enhance the thermoelectric properties for applications. For instance, the edge disorder[14] has been predicted theoretically to suppress greatly heat conductance of GNRs and high ZT can be achieved in the diffusive limit. The thermoelectric properties of graphene-based antidot lattices[15] are systematically investigated and the thermoelectric figure of merit (ZT) have been remarkably enhanced in such systems. Similarly, the point defects[12,16] and doping of isotopes[17,18] are also powerful approaches to considerably reduce the thermal conductivity. Besides the reduction of thermal conductance, the approach to boost the Seebeck coefficient S by the resonance and antiresonance in the electronic transport has been utilized for high thermoelectric properties. Recently, by taking advantage of the resonant tunneling of electrons, Mazzamuto *et al.*[11] showed that the mixed GNRs have high ZT at room temperature.

In this paper, we investigate the influence of the bended GNRs on the phonon and electron transport in ballistic region. We find that the electron resonant tunneling effect or the

*Project supported by the National Natural Science Foundation of China (Grant No. 61401153) and the Natural Science Foundation of Hunan Province, China (Grant Nos. 2015JJ2050 and 14JJ3126).

†Corresponding author. E-mail: hejun@hnu.edu.cn; panchangning2000@sina.com

© 2016 Chinese Physical Society and IOP Publishing Ltd

electron-wave quantum interference effect occurs in different quantum structures. These effects can be tuned by such kind of structure, so that the magnitude of the Seebeck coefficient can be regulated by the structure parameters. The enhanced Seebeck coefficient can be obtained. Combined with the dramatical reduction of the thermal conductance, the high values of ZT are then achieved for a certain kind of bended GNRs. Moreover, the resulting thermoelectric properties are highly dependent on the edge shapes and lengths of the assembled GNRs in such system. It leads the thermoelectric effect to be tunable. Such tunability will be helpful for designing and fabrication of high-performance thermoelectric devices such as ultrasensitive nanothermocouples.

2. Model and formulation

The simulated structures are schematized in Fig. 1. They all consist of two double-bend GNRs section, which act as central scattering zone, coupled with two semi-infinite leads with the same structure. The midsections are composed of armchair- or zigzag-edged GNR sectors linked alternatively. According to the edge shapes of the leads, we classify the devices into bended ZZ-GNRs (as shown in Fig. 1(a)) and bended AA-GNRs (as shown in Fig. 1(b)). The parameters

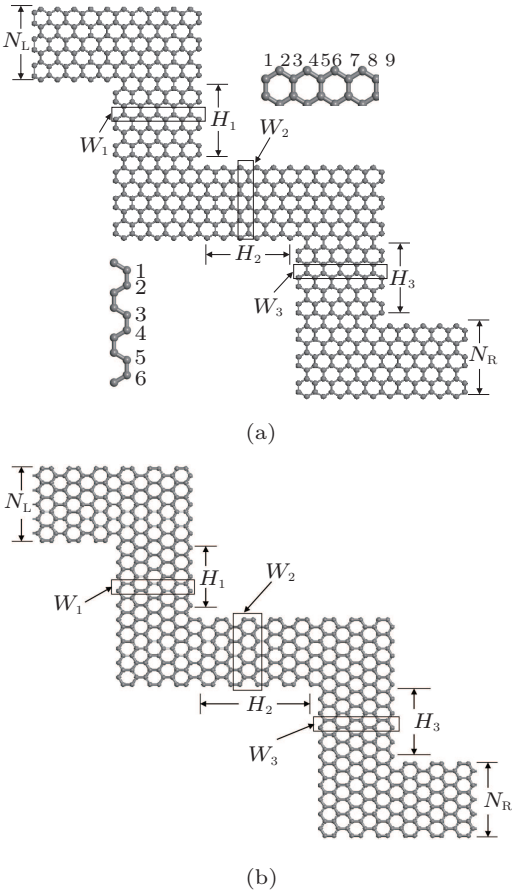


Fig. 1. Schematic diagram of the graphene nanoribbons: (a) bended ZZ-GNRs; (b) bended AA-GNRs.

W_n $(n = 1,2,3)$ are the lateral and longitudinal width of the midsections, H_n $(n = 1,2,3)$ are the interbend length, and the width of the left and right leads are described by N_L and N_R, respectively. All of the notation about the armchair- or zigzag-edged ribbons are the same as those in Ref. [19] (see the inset of Fig. 1).

For the simulation of phonon and electron transport in the graphene devices, we employ the powerful nonequilibrium Green's function (NEGF)[20] as a parallel way to calculate both the phonon and electron transmission functions T_e and T_{ph}. The force constant model including the fourth nearest neighbors is utilized for phonons, while the nearest-neighbor π-orbital tight-binding Hamiltonian is considered for electrons.[21,22] Generally, the NEGF approach can include the higher-order terms to consider decoherence effects coming from the electron–phonon and phonon–phonon interaction. However, due to the weak electron–phonon coupling and large phonon mean-free path in graphene, the electron–phonon and phonon–phonon interaction are neglected in this work.[15] The transmission function for electron is given by

$$T_e(E) = \mathrm{Tr}(\boldsymbol{G}^r \boldsymbol{\Gamma}_L \boldsymbol{G}^a \boldsymbol{\Gamma}_R). \tag{2}$$

Here the broadening function of the left (right) semi-infinite lead is $\boldsymbol{\Gamma}_{L(R)} = \mathrm{i}[\boldsymbol{\Sigma}^r_{L(R)} - \boldsymbol{\Sigma}^a_{L(R)}]$ with retarded self-energy of the leads $\boldsymbol{\Sigma}^a_{L(R)} = \boldsymbol{\Sigma}^r_{L(R)}{}^\dagger$, and the advanced Green's function $\boldsymbol{G}^a = (\boldsymbol{G}^r)^\dagger$. After introducing an intermediate function

$$\mathscr{L}^{(m)} = \frac{2}{h}\int_{-\infty}^{\infty}(E-\mu)^m\left[-\frac{\partial f(E,\mu,T)}{\partial E}\right]T_e(E)\,\mathrm{d}E, \tag{3}$$

where $f(E,\mu,T) = 1/(\mathrm{e}^{(E-\mu)/k_BT}+1)$ is the Fermi–Dirac distribution of the left/right lead at the chemical potential μ, which is also temperature dependent, the electronic quantities for calculation of the ZT can be presented as follows: the Seebeck coefficient

$$S = -\frac{1}{eT}\frac{\mathscr{L}^{(1)}}{\mathscr{L}^{(0)}},$$

the conductance $G = e^2\mathscr{L}^{(0)}$, and the electron thermal conductance

$$\kappa_e = \frac{1}{T}\left[\mathscr{L}^{(2)} - \frac{(\mathscr{L}^{(1)})^2}{\mathscr{L}^{(0)}}\right].$$

We can calculate the phonon transmission function in a similar way to the electronic transmission, and the corresponding phonon thermal conductance can be obtained as follows:[20–22]

$$\kappa_{ph} = \frac{\hbar^2}{2\pi k_B T^2}\int_0^\infty \nu^2 \frac{\mathrm{e}^{\hbar\nu/k_BT}}{(\mathrm{e}^{\hbar\nu/k_BT}-1)^2}T_{ph}(\nu)\,\mathrm{d}\nu. \tag{4}$$

3. Numerical results and discussion

Firstly, we investigate the thermoelectric properties of the bended ZZ-GNRs. The system is composed of the hybridized ZGNRs and AGNRs (see Fig. 1(a)). We take the

width $N_{L,R} = 7$, $W_1 = W_3 = 9$, $W_2 = 7$, the interbend length $H_1 = H_2 = H_3 = 8$. Figures 2(a) and 2(b) depict the transmission spectrum and thermal conductance of the phonon for the above structure and its straight counterpart 7-ZGNR, respectively. From Fig. 2(a), we can note that, regardless of the bended and straight structures, the phonon transmissions arise from the quantum value 3 in the limit $v \to 0$ due to the perfect transport of three acoustic phonons.

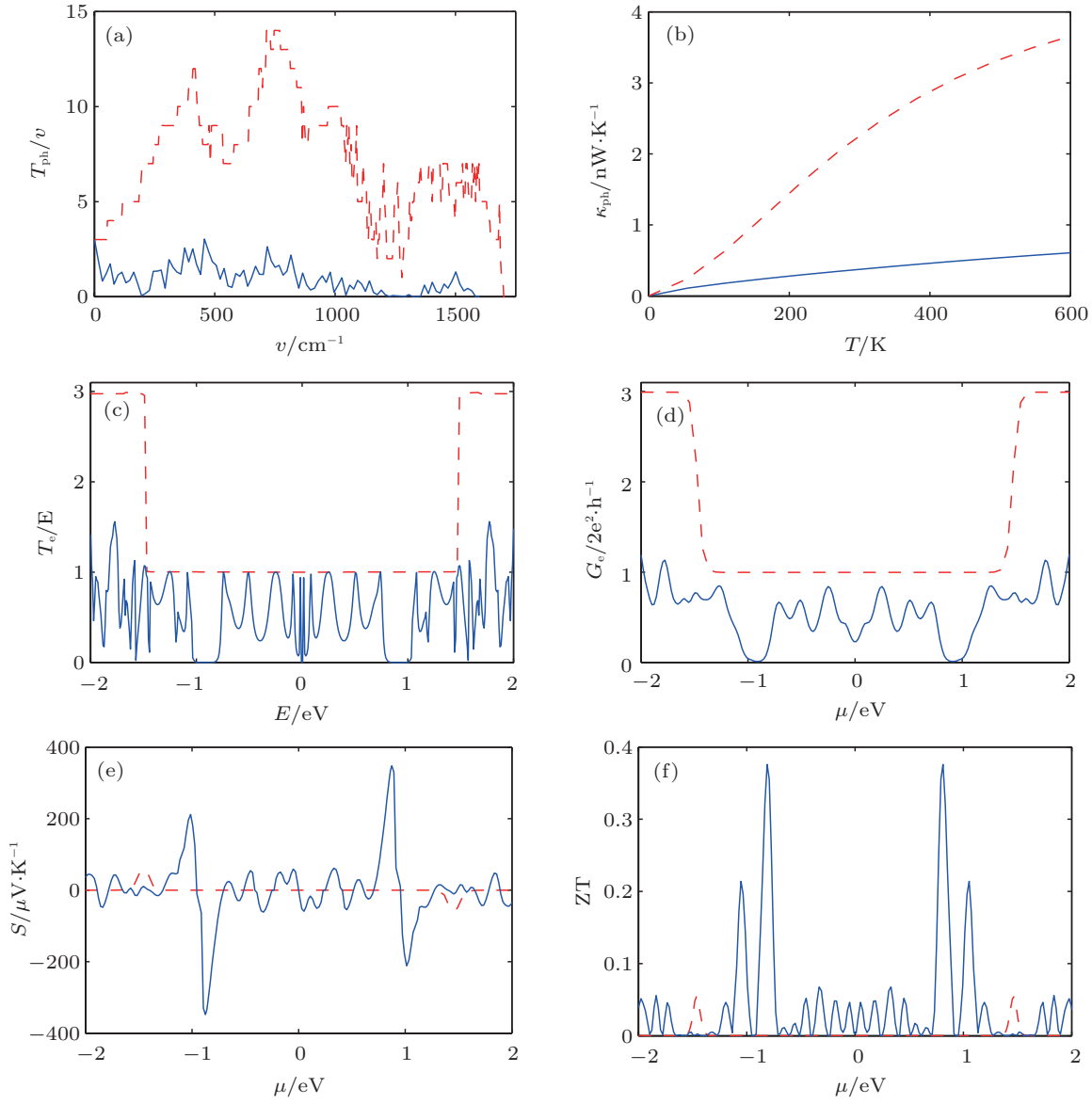


Fig. 2. (color online) Thermoelectric physical quantities for bended ZZ-GNRs (solid line) with $N_{L,R} = 7$, $W_1 = W_3 = 9$, $W_2 = 7$, $H_1 = H_2 = H_3 = 8$, and the straight 7-ZGNR (dashed line): (a) phonon transmission functions, (b) thermal conductance κ_{ph}, (c) electron transmission functions T_e, (d) electrical conductance G_e, (e) Seebeck coefficient S, and (f) thermoelectric figure of merit ZT versus chemical potential μ at temperature $T = 300$ K.

However, it can be clearly seen that such transmissions of phonon are suppressed significantly throughout the other frequency in the bended ZZ-GNR. Particularly, the phonon transport almost has been fully forbidden in the range of frequency from $v = 1220$ cm^{-1} to $v = 1340$ cm^{-1}. Therefore, the thermal conductance degrades considerably and is substantially lower than the straight 7-ZGNR with the same width (as shown in Fig. 2(b)). For instance, at room temperature $T = 300$ K, the thermal conductance is 0.38 nW/K for bended ZZ-GNR, which is 5–6 times fewer than that of the straight 7-ZGNR (about 2.3 nW/K). Furthermore, owing to the greater suppression effect of higher frequency phonon modes, the difference of phonon thermal conductance between the bended ZZ-GNR and the straight 7-ZGNR grows with the increase in temperature. Such spectacular suppression of phonon transmission and corresponding reduction of thermal conductance stem from the mismatch of phonon modes and the intense scattering effect between the ZGNR and AGNR linked sectors. In Figs. 2(c) and 2(d), we present the electron transmission properties T_e versus the energy E and the electron conductance G_e versus chemical potential μ. As we know, the straight 7-ZGNR with the zero bandgap exhibits metallic behavior, and

the straight 7-AGNR presents the semiconducting properties with a bandgap of about 1.4 eV. While for the studied system, due to the electronic resonant tunneling effect,[11] the multiple resonant peaks are clearly seen in the total electron transmission spectacular as shown in Fig. 2(c). Some electrons can be transported perfectly through the band-gap 7-AGNRs by this resonant tunneling effect, and the transmission coefficient reaches unity as the straight 7-ZGNR. However, the electron transmission is still close to zero for some energy ranges because of the existing of the bandgap of 7-AGNR. Similarly, such oscillations also occur in the conductance G_e as shown in Fig. 2(d). The multiple peaks of electron transmission result in the conductance resonant peaks, so that the high conductances have been preserved for some chemical potential μ. These oscillations originate from the specific geometry structure. In the given system, the ribbon sections with armchair edges are connected alternately in the zigzag nanoribbons which always present metallic properties. Because of the semiconducting properties, the armchair ribbon sections induce a band gap opening. While for the zigzag sections, it generates gapless edge localized states. So the sandwiched armchair sections can be seen as barriers between the metallic electron channel. The whole bended ZZ-GNRs can be considered as a multibarrier system. Hence, the structures give rise to very specific electron transport properties, and the resonant tunneling phenomena occur and induce strong oscillations of the conductance. In addition, the Seebeck coefficient S is determined by the electron-transmission-weighted average value of the energy $E-\mu$.[12] For the straight ZGNR, the metallic behaviors with the symmetric transmission around the Fermi level lead to the very small peak value of $S \sim 50$ μV/K near the first conductance band (FCB), resulting in a very small ZT ~ 0.06 as shown in Figs. 2(e) and 2(f). However, the large fluctuations emerge in the Seebeck coefficient curve within the FCB and the peak value reaches $S \sim 350$ μV/K. It stems from the contributions of the oscillations of the electronic transmission. Because the Seebeck coefficient S is related to the logarithmic derivative of the electronic transmission, i.e., $S(T,\mu) \approx (\pi^2 k_B^2 T/3e)(\partial \ln T_e/\partial E)\,|_\mu$,[11,15] large numerical fluctuations of the electronic transmission will correspond to the large logarithmic derivative and result in the high Seebeck coefficient (Fig. 2(e)). That is to say, the resonant tunneling transport of electron enhances the Seebeck coefficient S. As expected, the high Seebeck coefficient, combined with the suppression of lattice thermal conductance, yield the high thermoelectric figure of merit ZT. The first peak of $ZT_{max} = 0.38$ is obtained at $\mu = 0.81$ eV for this system, which is strongly boosted, compared to the straight 7-ZGNRs with $ZT_{max} = 0.05$ at $\mu = 1.46$ eV (see Fig. 2(f)). Meanwhile, we find that the ZT_{max} is very sensitive to the chemical potential. The second peak of ZT $= 0.21$ occurs at $\mu = 1.05$ eV. It may add some complexity of the usefulness of the system as a robust thermoelectric device.

Now, we turn to study thermoelectric properties of the bended AA-GNRs (see Fig. 1(b)). In contrast to metallic ZGNRs, AGNRs can exhibit the semiconducting or metallic properties with the dependence on the width. Hence, we must discuss both semiconducting and metallic AGNRs leads, respectively. For the metallic AGNRs leads, the width of armchair-edge graphene sections $N_{L,R} = W_2 = 5$ are taken to keep the gapless properties, and $W_1 = W_3 = 6$ with the metallic zigzag-edge graphene sections, the interbend length $H_1 = H_3 = 25$, and $H_2 = 10$. Figure 3(a) depicts the phonon transmission as a function of the phonon model frequency ν for the bended AA-GNR and the straight counterpart 5-AGNR. We note that, similarly to the ZZ-GNR, the phonon transmission has also been substantially suppressed due to the mismatch of the phonon modes in the center scattering sections. As a result, the corresponding thermal conductance is substantially lower than the straight 5-AGNR. At room temperature, the straight 5-AGNR has a thermal conductance of 0.8 nW/K, while the bended AA-GNR's thermal conductance decreases to 0.2 nW/K as shown in Fig. 3(b). The total electronic transmission probability is depicted as a function of energy for such system (see Fig. 3(c)). Because of the metallic behavior of AGNRs, the whole structure forms a metallic–metallic link. However, it is important to note that, due to the quantum interference effect of electron transport in the system,[24,25] the oscillation phenomenon also occurs within the FCB. Many peaks come into being in the electron transport. For instance, the incident electrons with energies of about 0.6 eV, 0.9 eV, and 1.1 eV can transport perfectly as the straight 5-AGNR. In addition to the electron transport peaks, we also find that incident electrons with energies within 1.4 eV–1.5 eV are totally reflected and give rise to the electron transport gap. This large antiresonance gap in the transmission probability is the result of the quantum interference of electron waves caused by the mode mismatch.[25–28] Hence, the physical mechanism of the electron transport is different from the above electronic resonant tunneling effect of the ZZ-GNR. Furthermore, these antiresonance gaps and resonance peaks lead to the oscillations of the conductance G_e as shown in Fig. 3(d), so that high magnitudes of G_e remain constant at the corresponding chemical potential. Similarly, since the Seebeck coefficient S is proportional to the logarithmic derivative of the electronic transmission. The peak values of the Seebeck coefficient S always occur near the edge of antiresonance gap. As shown in Fig. 3(e), the largest Seebeck coefficient $S \sim 200$ μV/K occurs at lower edge of the gap, which is considerably larger than the straight 5-AGNR with only about 35 μV/K. The large Seebeck coefficient S, combined with the reduced phonon thermal conductance and preserved electronic conductance, result in many

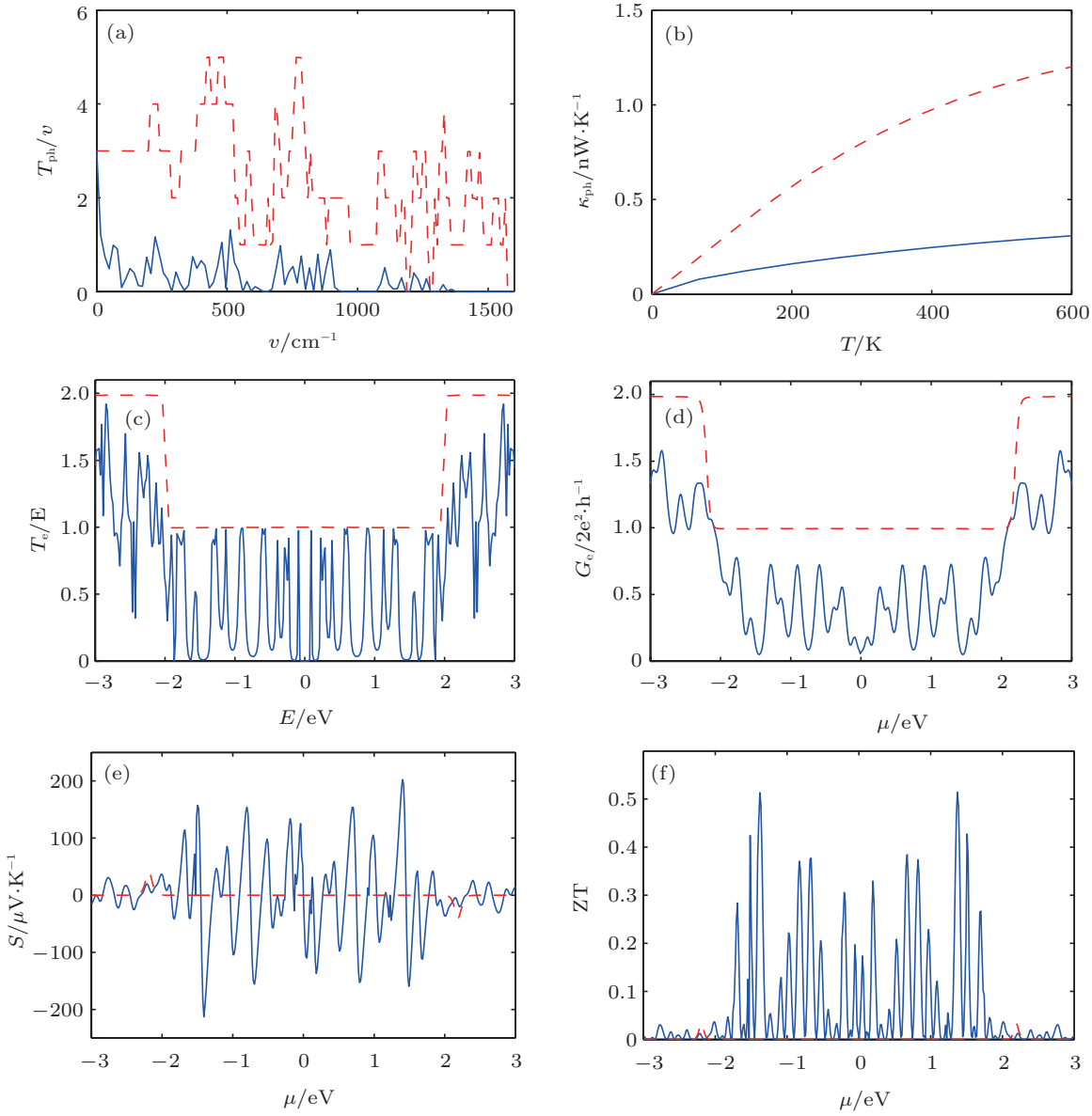


Fig. 3. (color online) Thermoelectric physical quantities for bended AA-GNRs (solid line) with $N_{L,R} = 5$, $W_1 = W_3 = 6$, $W_2 = 5$, $H_1 = H_3 = 25$, $H_2 = 10$, and the straight 5-AGNR (dashed line): (a) phonon transmission functions, (b) thermal conductance κ_{ph}, (c) electron transmission functions T_e, (d) electrical conductance G_e, (e) Seebeck coefficient S, and (f) thermoelectric figure of merit ZT versus chemical potential μ at temperature $T = 300$ K.

peak values of the figure of merit ZT, and the maximum peak value $ZT_{max} = 0.53$ can be obtained at $\mu = 1.38$ eV. Compared to the corresponding 5-AGNR with $ZT_{max} = 0.03$, the thermoelectric properties have been increased by more than ten times.

For the semiconducting leads AA-GNRs, the thermoelectric properties are different from the metallic leads AA-GNRs owing to the opened gap. Here, we take the width $N_{L,R} = 7$, $W_1 = W_3 = 6$, $W_2 = 5$, and the interbend length $H_1 = H_3 = 25$, $H_2 = 25$. The thermoelectric properties are shown in Fig. 4. From Fig. 4(b), we find that the thermal conductance κ_{ph} increases due to the wider leads. For electron transport, the total transmission keeps the band gap as the straight semiconducting 7-AGNR ranges from -0.75 eV to 0.75 eV. However, as same as the above metallic leads, the quantum interference effect of electron transport also appears and the oscillation phenomenon occurs within the FCB. The electrical conductance G_e also presents some oscillations. These oscillations greatly strengthen the figure of merit and leads to $ZT_{max} = 0.63$ at room temperature $T = 300$ K, as shown in Fig. 4(f).

The calculations above clearly demonstrate that the bended graphene nanoribbons have superior thermoelectric performance compared to the straight nanoribbons. It is found that the thermal conductance is greatly affected by the variation of the geometry in the bended graphene nanoribbons, and electronic transport properties are very sensitive to the geometry parameters as well. Owing to the dependence of the ZT on both thermal conductance and electronic conductance, it exhibits very complex relations to the geometry parameters. Meanwhile, structure-sensitive properties indicate that the figure of merit ZT is tunable and provides an effective method for designing controllable thermoelectric devices. Therefore, it is

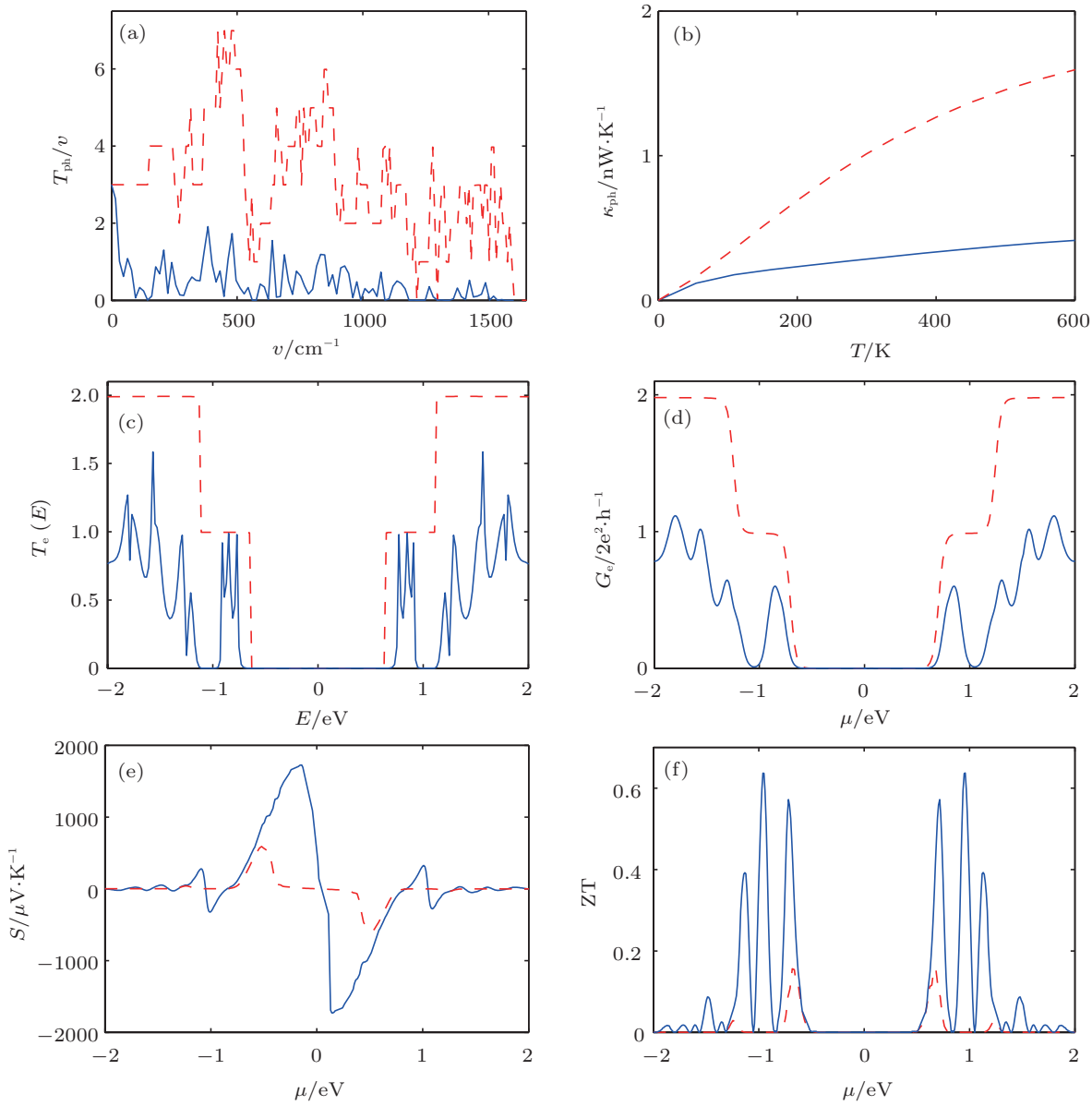


Fig. 4. (color online) Thermoelectric physical quantities for bended AA-GNRs (solid line) with $N_{L,R} = 7$, $W_1 = W_3 = 6$, $W_2 = 7$, $H_1 = H_3 = 25$, $H_2 = 10$, and the straight 7-AGNR (dashed line): (a) phonon transmission functions, (b) thermal conductance κ_{ph}, (c) electron transmission functions T_e, (d) electrical conductance G_e, (e) Seebeck coefficient S, (f) thermoelectric figure of merit ZT versus chemical potential μ at temperature $T = 300$ K.

of great importance to investigate systematically the geometry influences to the ZT_{max} in the presented system. The ZT_{max} values varying with respect to the interbend length H_1 and H_3 have been plotted for both bended ZZ-GNRs (see Fig. 5(a)) and AA-GNRs (see Fig. 5(b)) at the temperature $T = 100$ K, 300 K, and 600 K, where other parameters are similar to the above-mentioned structure except for $H_{1,3}$. It is shown that the ZT_{max} values always increase with the interbend length H_1 and H_3 for ZZ-GNRs, although only slightly increase for $H_1 = H_3 = 2, 4, 6$. The ZT_{max} can be tuned from 0.05 to 0.38. Nevertheless, for the AA-GNRs, slight oscillations of ZT_{max} are also found in the overall upward tendency. For instance, the $ZT_{max} = 0.39$ for $H_1 = H_3 = 20$ is a little less than $ZT_{max} = 0.41$ for $H_1 = H_3 = 15$ at room temperature. The reason is that the quantum interference effect occurs in the electron transport. It gives rise to some fluctuations in the transport curve. The peaks of T_e occur at different energy E and the peak values are different for such systems. Thus the small oscillations appear. It indicates that the ZT_{max} of AA-GNRs have more complex dependence on the geometry parameters. When $H_1 = H_3 = 30$, we find that $ZT_{max} = 0.63$ and 0.72 can be achieved at temperature $T = 300$ K and $T = 600$ K, respectively. Thermoelectric properties are substantially improved by the quantum interference effect of electron transport. According to the definition, ZT is a function of T, G_e, S, κ_e, and κ_{ph}. Unfortunately, these physical quantities are closely related to the carrier concentration and lattice temperature. One physical parameter often adversely affects another. Particularly, the transmission of electron is very sensitive to the parameter H_1 and H_3. Thus, for higher H_1 and H_3, the ZT has a little change, even a small decrease occurs due to the effect of electronic transport. In addition, with the increase of the width

of N_L, N_R, W_1, W_2, and W_3, the phonon thermal conductance increases rapidly, which will decrease the value of ZT_{max} in our calculations.

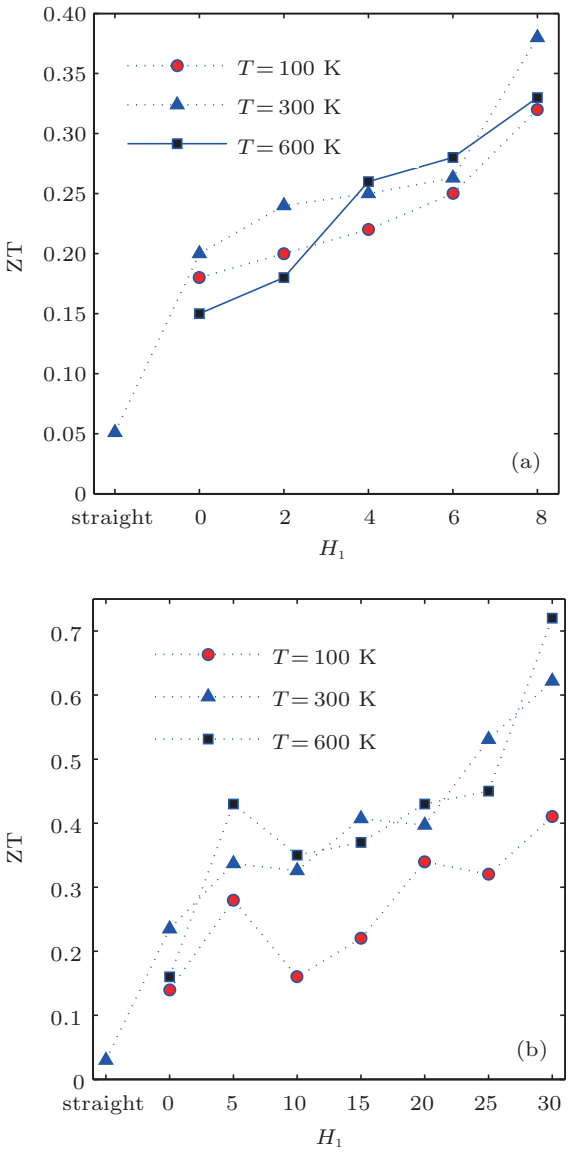


Fig. 5. (color online) The figure of merit ZT as a function of the interbend length H_1 and H_3 ($H_3 = H_1$) at temperature (T = 100 K, 300 K, and 600 K) for (a) bended ZZ-GNRs and (b) bended AA-GNRs, where other parameters are similar to that in Figs. 2 and 3, respectively.

4. Summary

We have presented an atomistic simulation of the ballistic thermoelectric properties for the bended GNRs. Compared with the straight GNR counterparts with the same width, the enhanced thermoelectric performance has been found in these systems. Such improvement originates from the combination of the reduction of phonon thermal conductance caused by the scattering of interface and the mismatch of phonon modes, and the high electronic conduction and Seebeck coefficient induced by the oscillations of electron transport. Meanwhile, we find that these transport oscillations stem from different physical mechanisms, i.e., the electron resonant tunneling effect for ZZ-AGNRs and quantum interference effect of electron transport for AA-GNRs. The dependence of structural parameters of ZT_{max} in bended ZZ/AA-GNRs have also been systematically investigated. We found that the thermoelectric effect could be conveniently tuned by the interbend length. The geometry-controlled ballistic thermoelectric effect provides a guideline for the design of thermoelectric devices such as graphene-based thermocouples.

References

[1] Zhang Y B, Tan Y W, Stormer H L and Kim P 2005 *Nature* **438** 201
[2] Geim A K 2009 *Science* **324** 1530
[3] Wang Q, Xie H Q, Jiao H J, Li Z J and Nie Y H 2012 *Chin. Phys. B* **21** 117310
[4] Wu Z H, Xie H Q, Zhai Y B, Gan L H and Liu J 2015 *Chin. Phys. B* **24** 034402
[5] Yu Z, Guo Y, Zheng J and Chi F 2013 *Chin. Phys. B* **22** 117303
[6] Feng S K, Li S M and Fu H Z 2014 *Chin. Phys. B* **23** 117202
[7] Guo H H, Yang T, Tao P and Zhang Z D 2014 *Chin. Phys. B* **23** 017201
[8] Xue L, Xu B and Yi L 2014 *Chin. Phys. B* **23** 037103
[9] Kim R, Datta S and Lundstrom M S 2009 *J. Appl. Phys.* **105** 034506
[10] Zhou J and Yang R G 2011 *Appl. Phys. Lett.* **98** 173107
[11] Mazzamuto F, Nguyen V H, Apertet Y, Caër C, Chassat C, Martin J S and Dollfus P 2011 *Phys. Rev. B* **83** 235426
[12] Ouyang Y and Guo J 2009 *Appl. Phys. Lett.* **94** 263107
[13] Seol J H, Jo I, Moore A L, Lindsay L, Aitken Z H, Pettes M T, Li X, Yao Z, Huang R, Broido D, Mingo N, Ruoff R S and Shi L 2010 *Science* **328** 213
[14] Li W, Sevincli H, Cuniberti G and Roche S 2010 *Phys. Rev. B* **82** 041410
[15] Gunst T, Markussen T, Jauho A P and Brandbyge M 2011 *Phys. Rev. B* **84** 155449
[16] Chang P H and Nikolić B K 2012 *Phys. Rev. B* **86** 041406
[17] Jiang J W, Lan J H, Wang J S and Li B W 2010 *J. Appl. Phys.* **107** 054314
[18] Hu J, Schiffli S, Vallabhaneni A, Ruan X and Chen Y P 2010 *Appl. Phys. Lett.* **97** 133107
[19] Xu Y, Chen X B, Gu B L and Duan W H 2009 *Appl. Phys. Lett.* **95** 233116
[20] Wang J S, Wang J and Lü J T 2008 *Eur. Phys. J. B* **62** 381
[21] Jiang J W, Wang J S and Li B W 2011 *J. Appl. Phys.* **109** 014326
[22] Pan C N, Xie Z X, Tang L M and Chen K Q 2012 *Appl. Phys. Lett.* **101** 103115
[23] Wu Y and Yang X X 1997 *Phys. Rev. Lett.* **78** 3086
[24] Shi Q W, Zhou J and Wu M W 2004 *Appl. Phys. Lett.* **85** 2547
[25] Weisshaar A, Lary J, Goodnick S M and Tripathi V K 1989 *Appl. Phys. Lett.* **55** 2114
[26] Nie Y H, Zhang Y B, Liang J Q, *et al.* 1999 *Physica B: Condensed Matter* **270** 95
[27] Nie Y H, Jin Y H, Liang J Q, *et al.* 2000 *J. Phys.: Conden. Matt.* **12** L87
[28] Li X Q and Yan Y J 2001 *Appl. Phys. Lett.* **79** 2190